THEORY, SIMULATION, AND EXPERIMENT OF A SINGLE MODULE COAX-TO-PARALLEL-PLATE TRANSITION FOR THE TRANSFORMER SECTION OF PBFA II

William A. Johnson, Larry X. Schneider, Eugene L. Neau
Sandia National Laboratories
P. O. Box 5800
Albuquerque, New Mexico 87185

SAND--89-1494C

DE89 013493

Introduction

Techniques are being developed to gain understanding of energy transport efficiencies through changes in pulsed power transmission line geometries. These techniques are being applied to a design study of the PBFA-II accelerator which has the goal of increasing the energy available for ICF experiments.

Transverse electromagnetic (TEM) wave analysis yields a simple circuit model of the new coax-to-parallel-plate transition. This simple model gives insight into the dominant physics of the device and suggests design improvements that will lead to the desired energy efficiencies. Insights gained by this simple model are confirmed and refined by 3-dimensional, time dependent computer simulations with the SOS code[1] and scale model experiments. Simulations have predicted experimental results to a high degree of accuracy which adds confidence in both the simulations and the scale model experiments.

Figure 1 illustrates the geometry of the coax-to-parallel plate transition. This design evolved from the following observations about the present transformer section of PBFA II: the crossover region of the transformer section (Fig. 2) is merely a lossy transformer which converts two main lines in parallel into two main lines in series; as the gap between these parallel plates increases, energy flows from the main lines to the exterior regions. Thus, the new configuration employs disks in an attempt to confine the energy to the main lines. Theoretically, it is desirable to allow the transition from the coax-to-disk sector to occur over a distance whose transit time is large compared to the duration of the input pulse, in order to avoid the excitation of higher order modes. However, space limitations constrain the transition to be abrupt. Figure 3a illustrates the geometry of the new transition.

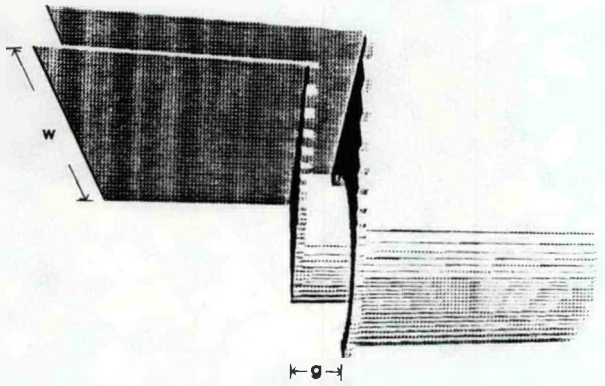

Figure 1. Geometry of the coax-to-parallel-plate transition.

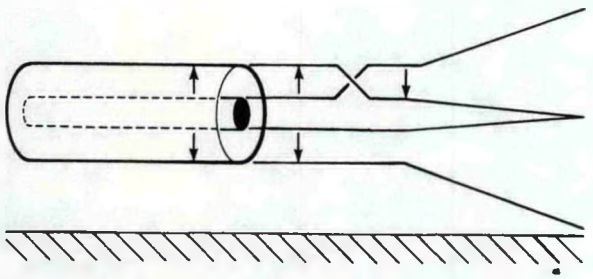

Figure 2. The present PBFA-II configuration has a crossover section that acts like an abrupt impedance transformation. Furthermore, as the gaps between the parallel plates increase energy flows to the exterior of the main lines.

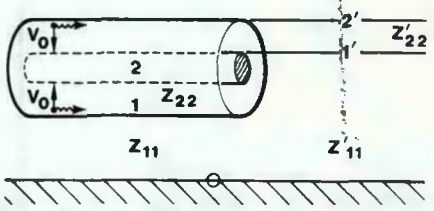

Figure 3. (a) The coax-to-parallel-plate transition.

TEM analysis yields a simple circuit model for the new transition as well as the expression

$$E_{eff} = \left(\frac{\frac{2}{Z_{22}}}{\frac{1}{Z_{22}} + \frac{1}{Z'_{22}} + \frac{1}{Z_{11} + Z'_{11}}} \right)^2 \frac{Z_{22}}{Z'_{22}} \qquad (1)$$

for the energy efficiency of the transition. Figure 3b illustrates the circuit model of the new transition. Optimizing the energy flow into the main parallel plate line requires that Z'_{22} be matched to Z_{22} and that the sum $Z_{11} + Z'_{11}$ be made infinite.

In order to raise the external impedance Z'_{11}, a layer of plastic is placed on the floor as shown in Fig. 4. The region exterior to this plastic ($\varepsilon_r = 3$) is water filled ($\varepsilon_r = 81$). The water and plastic regions are in series, thus

$$C = \frac{\varepsilon_0}{\frac{d_1}{81w} + \frac{d_2}{3w}} \qquad (2a)$$

$$L = \frac{d\,\mu_0}{w} \qquad (2b)$$

$$Z'_{11} = \sqrt{L/C} \qquad (2c)$$

where w is the plate width, and ε_0 and μ_0 are respectively the permittivity and permeability of free space. The improvement in efficiency due to the increase in Z'_{11} may be offset by shorting out of the junction, if the short at the end of the exterior line (Fig. 4) is not transit-time isolated from the junction. The velocity of the TEM wave in this exterior region is given by

$$V_{TEM} = \frac{1}{\sqrt{LC}} = c\sqrt{\frac{d_1}{81d} + \frac{d_2}{3d}} \qquad (3)$$

where c is the velocity of light in vacuum. To insure transit-time isolation between the junction and short in Fig. 4 for the duration of the pulse, 10% of the exterior region is filled with plastic. If more plastic is added, reflections from the short begin to reach the junction during the duration of the pulse.

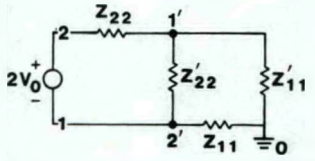

Figure 3. (b) TEM analysis yields this simple circuit model.

* This work supported by the U.S. Department of Energy under Contract No. DE-AC04-76-DP00789.

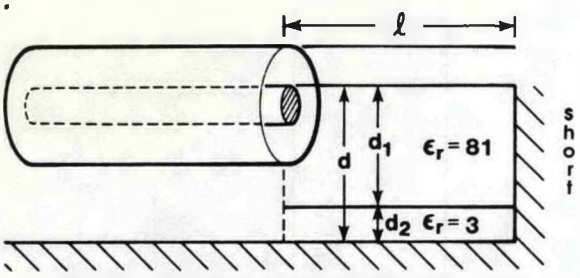

Figure 4. A layer of plastic raises the external impedance in the parallel-plate region. The amount of plastic is chosen to maximize this impedance while insuring transit time isolation between the short and the junction for the duration of the pulse. The two-way transit distance (2ℓ) is 6 m and the pulse duration is 100 ns for PBFA II. This corresponds to 1 m and 16.7 ns respectively for the scale model.

Figure 5 illustrates the one-sixth scale, single-module model. To approximate the mirror symmetry planes which occur in PBFA II, plastic side walls have been used in this water-filled tank. The high contrast between the relative dielectric constants of water and plastic ($81 >> 3$) makes this a good approximation. Figure 6 shows the probe locations in the scale model. Time-dependent, three-dimensional, computer simulations of this geometry have been carried out.

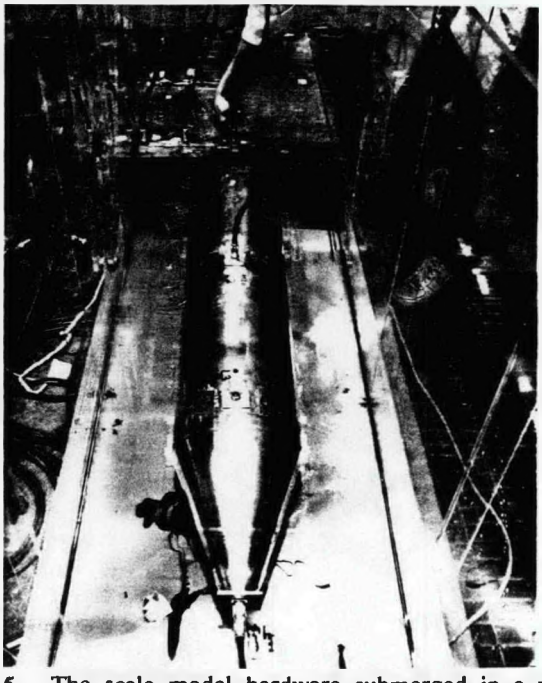

Figure 5. The scale model hardware submerged in a water filled plastic tank. The plastic walls were used to approximate the mirror symmetry planes of PBFA II. The water-plastic interface is a good approximation to a mirror symmetry plane because the relative dielectric constant of water is much greater than the relative dielectric constant of the plastic.

Table 1 gives results of TEM analysis and 3-dimensional computer simulations of this scale, single-module model. The energy efficiencies include a 100 ns (16.7 ns for the 1/6 scale model) time window after which it is assumed that the plasma opening switch will open and the energy will be transferred to the diode. The discrepancy between the TEM analysis and the 3-D computer simulations is attributed to the excitation of higher-order modes by the junction. When plastic is placed in the junction, the junction transit times are greatly reduced and one would expect a corresponding decrease in higher order mode excitation. As seen in Table 1 by the excellent agreement between TEM analysis and computer simulation, the

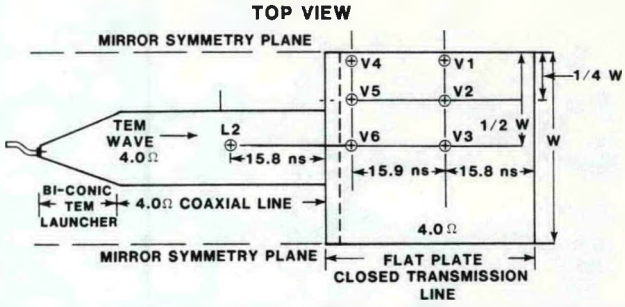

Figure 6. Geometry of the scale model experiment with probe locations. The transit time from the beginning of the junction to V6 is 3 ns in water.

Table 1. A comparison of energy efficiencies computed by TEM analysis and 3-dimensional computer simulations for the scale model experiment.

	TEM	SOS
ALL WATER	0.77	0.69
2.54cm PLASTIC ON FLOOR	0.87	0.78
2.54cm PLASTIC ON FLOOR FLOOR AND PLASTIC IN JUNCTION	0.87	0.85

energy in the higher-order modes is also greatly reduced by placing plastic in the junction.

Comparison with Experimental Data

Understanding of the propagating higher order modes yields insight into both the computer simulations and experimental results. Figure 7a illustrates the geometry of the parallel plate-lines. Mirror symmetry planes correspond to the approximate PBFA-II environment, neglecting the pie-section shape of a single module, and approximate the water-plastic interface at the side walls in the scale model experiment. Transverse electric waves may propagate in this structure. The $TE_{o,m}$ mode is described in the frequency domain, with an $e^{j\omega t}$ time dependence suppressed, by

$$H_z = (m\pi/w)\sin(m\pi y/w)\exp\left(-j\sqrt{k^2 - (m\pi/w)^2}\,z\right)$$

$$E_x = -j\omega\mu\cos(m\pi y/w)\exp\left(-j\sqrt{k^2 - (m\pi/w)^2}\,z\right) \qquad (4)$$

$$H_y = -j\sqrt{k^2 - (m\pi/w)^2}\cos(m\pi y/w)\exp\left(-j\sqrt{k^2 - (m\pi/w)^2}\,z\right).$$

Figure 7. (a) The geometry a parallel-plate line.

Figure 7b illustrates the voltage variations across the plates for the TEM ($m = 0$), $TE_{0,1}$, and $TE_{0,2}$ modes. Since both excitation and geometry is even about w/2 the odd mode is not excited. The plate width w for the scale model geometry is 0.612 m, thus the $m = 2$ mode has a cutoff frequency of 54 Mhz. The input pulse of the scale model experiment (Figs. 8a and 8b) has significant energy above this frequency. Since the cutoff frequencies of the other even higher order modes are located in regions ($f > 108$ Mhz) where the input pulse has little energy, they may be neglected. Thus, to accurately obtain TEM energy efficiencies in both computer simulations and experiments voltage monitors should be placed at the nulls

of the $TE_{0,2}$ mode. Probes located at peaks of this mode will measure the combinted voltage due to the TEM and $TE_{0,2}$ mode.

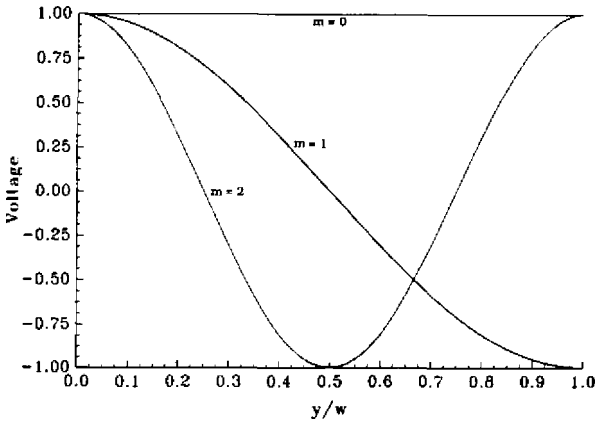

Figure 7. (b) Voltage variations across the line for the TEM, $TE_{0,1}$, and $TE_{0,2}$ modes.

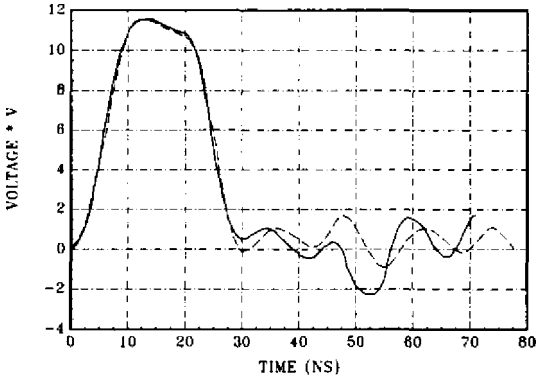

Figure 8. (a) The inlet voltage

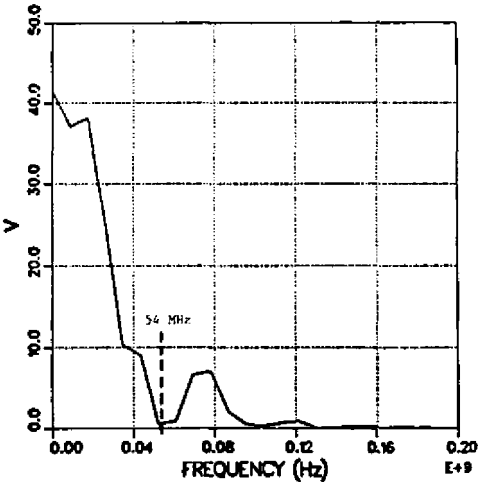

Figure 8. (b) its Fourier transform.

Figures 9a and 9b show voltage waveforms for a water-filled junction with a 2.54 cm gap without plastic on the floor. Figure 9a corresponds to the probe locations near the junction, while Fig. 9b corresponds to the down-line probe locations. As the wave propagates downline dispersion is evident at the non-TEM probe locations. This dispersion is indicative of the presence of the higher-order, non-TEM modes. The presence of higher-order modes in Fig. 9a is also apparent due to the difference between the TEM, center, and edge waveforms. It is further noted that from the odd symmetry of the $TE_{0,2}$ mode about the TEM probe location (Figs. 6 and 7b) that the

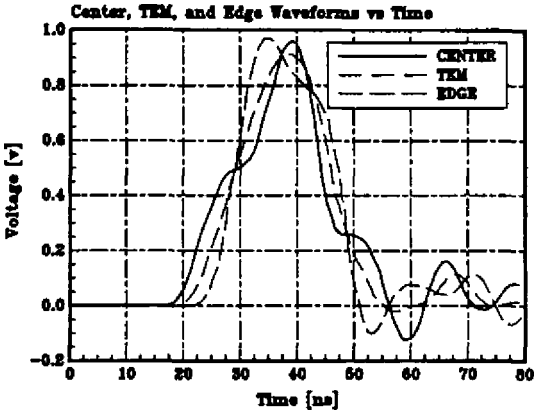

Figure 9. Scale model computer simulations for a 2.54 cm gap (Fig. 1) and a 2.54 cm layer of plastic on the floor.

(a) Voltage waveforms near the junction at locations center, TEM, and edge corresponding to V_6, V_5, and V_4 of Fig. 6.

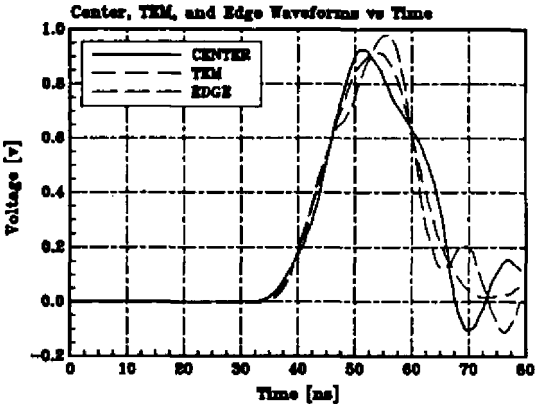

(b) The downline voltages at the center, TEM, and edge locations correspond to the probe locations V_3, V_2, and V_1, respectively in Fig. 6.

waveform shapes are to be expected. In Figs. 10a and 10b results are given for a 2.54 cm plastic filled junction with a 2.54 cm layer of plastic on the floor. The plastic in the junction has substantially reduced the amount of energy launched into the higher-order modes. To further reduce the higher-order-mode content thin, longitudinal slots have been placed at the H_z (J_y) peaks of the $TE_{0,2}$ and $TE_{0,4}$ modes on the top plate of the parallel plate section. Unfortunately the slots only dissipate the higher-order-mode energy, rather than converting it back into TEM mode energy.

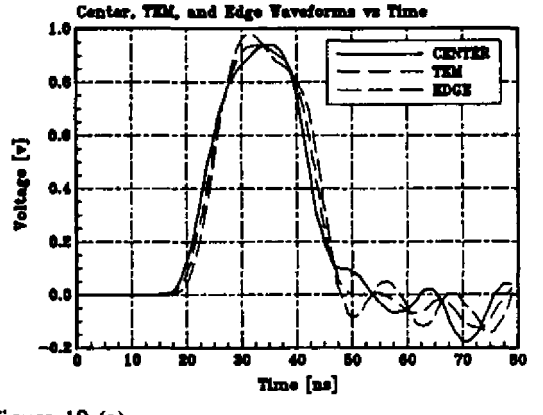

Figure 10 (a).

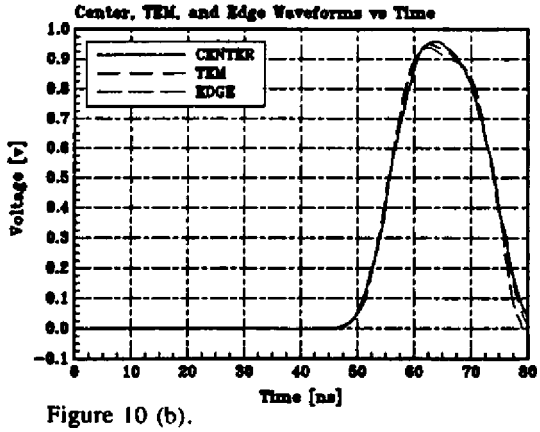

Figure 10 (b).

Figure 10. Scale model results for the geometry of Fig. 6, but with plastic filling the junction. To further attenuate higher order modes, thin longitudinal slots have been placed on the top plate of the parallel plate section at the peaks of H_z, for the $TE_{0,2}$ and $TE_{0,4}$ modes. To extract the TEM wave component the wave in (b) was allowed to propagate 29 ns downline from the probes located closest to the junction.

Comparisons of computer simulations and experimental results are shown in Figs. 11a-11d. Figure 11a shows the input waveforms measured in the coax while Figs. 11b-11d correspond to monitor locations V_1, V_2, and V_3 of Fig. 6.

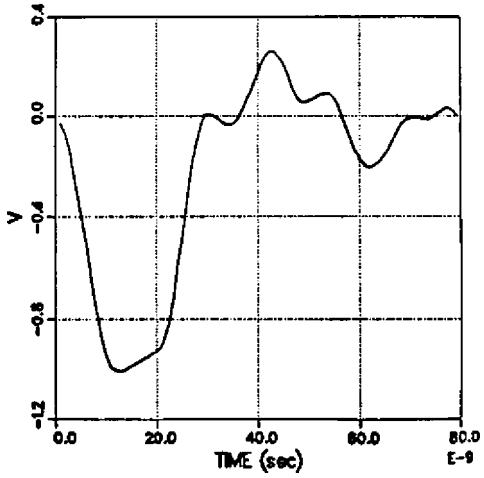

Figure 11 (a).

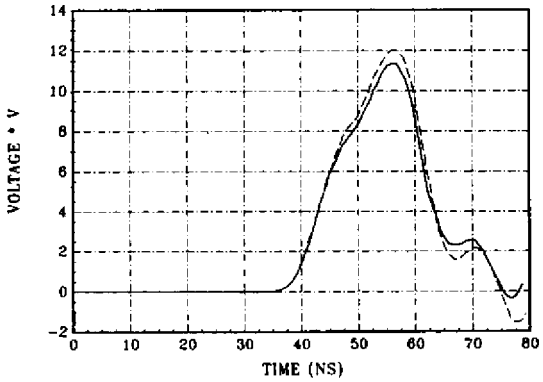

Figure 11 (b).

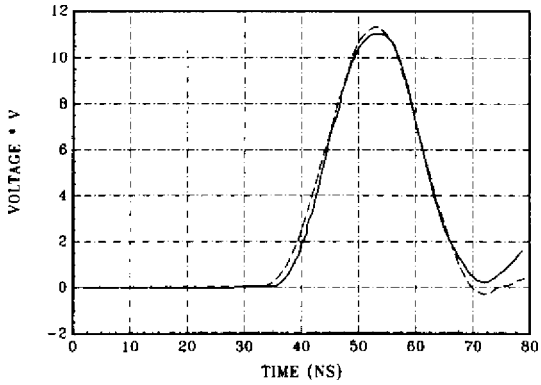

Figure 11 (c).

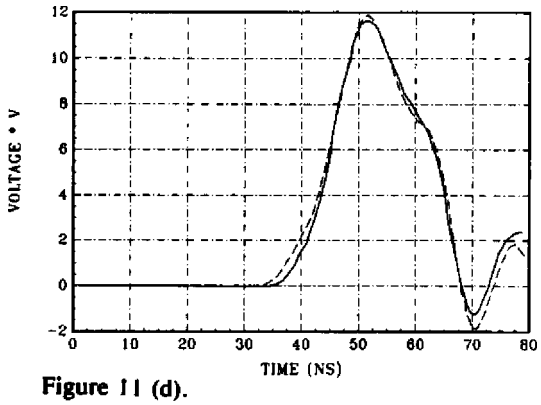

Figure 11 (d).

Figure 11. Comparison between computer simulations (---) and experiment (——) for the scale model experiment of Fig. 10 for the case of no plastic in the junction and 2.54 cm thick plastic on the floor in the parallel plate section. Figure 11a shows the input waveform measured in the coax while Figs. 11b, 11e, and 11d show waveforms measured at probe locations V_1, V_2, and V_3 of Fig. 6.

Summary

Although the simple, TEM analysis presented does not account for reflections beyond the junction, it remains valid throughout the time window of concern (the duration of input pulse). This TEM analysis also does not account for the energy lost to higher-order modes. However, it does give insight into the remaining physics of the coax-to-parallel-plate transition and by means of the simple circuit of Fig. 3b illustrates the major design constraints of this device. A further design constraint is to minimize the energy launched into higher-order modes. The efficiencies of Table I (>75%) indicate a potential gain of greater than 50% in energy-transport efficiency for PBFA II. However, this result does not account for multi-module, cross-coupling effects. Thus, this simple TEM analysis is currently being extended to account for multi-module effects.

Acknowledgements

The authors wish to acknowledge helpful discussions with L. K. Warne, D. B. Seidel, M. L. Kiefer, J. T. Crow, and T. L. Lockner. Further help with the scale model experiments from J. Puissant is gratefully acknowledged.

References

1. B. Goplen et al., "User's Manual for SOS," Mission Research Corp., September 1983.